EUROPEAN ORGANIZATION FOR NUCLEAR RESEARCH

Pseudorapidity densities of charged particles with transverse momentum thresholds in pp collisions at $\sqrt{s} = 5.02$ and $13\,\mathrm{TeV}$

ALICE Collaboration

Abstract

The pseudorapidity density of charged particles with minimum transverse momentum (p_T) thresholds of 0.15, 0.5, 1, and $2\,\mathrm{GeV}/c$ was measured in pp collisions at centre-of-mass energies of $\sqrt{s} = 5.02$ and $13\,\mathrm{TeV}$ with the ALICE detector. The study is carried out for inelastic collisions with at least one primary charged particle having a pseudorapidity (η) within ± 0.8 and p_T larger than the corresponding threshold. The measurements were also performed for inelastic and non-single-diffractive events as well as for inelastic events with at least one charged particle having $|\eta| < 1$ in pp collisions at $\sqrt{s} = 5.02\,\mathrm{TeV}$ for the first time at the LHC. The measurements are compared to the PYTHIA 6, PYTHIA 8, and EPOS-LHC models. In general, the models describe the pseudorapidity dependence of particle production well, however, discrepancies are observed for event classes including diffractive events and for the highest transverse momentum threshold ($p_\mathrm{T} > 2\,\mathrm{GeV}/c$), highlighting the importance of such measurements for tuning event generators. The new measurements agree within uncertainties with results from the ATLAS and CMS experiments.

1 Introduction

The pseudorapidity density of charged particles, $dN_{ch}/d\eta$, is a key observable for understanding the general properties of particle production in high-energy hadronic collisions. At collider energies, particle production in proton–proton (pp) collisions has origins in both soft and hard processes [1]. Hard processes are those with high enough transverse momentum transfer ($Q \gg \Lambda_{QCD} \sim 200$ MeV) between the scattering partons such that they can be described by perturbative quantum chromodynamics (pQCD) processes [2]. For the description of soft processes, non-perturbative phenomenological models inspired by pQCD and implemented in modern Monte Carlo generators are needed [3–11]. The measurement of the charged particle pseudorapidity density provides constraints on the descriptions of particle production mechanisms and input for tuning of Monte Carlo event generators, such as PYTHIA and EPOS used for physics at hadron colliders [8, 9, 12–15].

Following earlier ALICE studies of particle production in pp collisions [16–20], this publication presents a set of measurements of the pseudorapidity density of primary charged particles in inelastic events (INEL), non-single-diffractive events (NSD), and inelastic events with at least one charged particle in $|\eta| < 1$ (INEL>0) for pp collisions at $\sqrt{s} =$ 5.02 TeV. In ALICE, primary charged particles are defined as charged particles with a mean proper lifetime τ larger than 1 cm/c which were produced either promptly at the primary vertex or from decays of particles with $\tau < 1$ cm/c restricted to decay chains leading to the interaction [21]. In the previous measurements of Refs. [16–20], $dN_{ch}/d\eta$ was reported for the INEL, NSD, and INEL>0 event classes and without any selection on the transverse momentum (p_T) of the particles, i.e. for $p_T > 0$.

In order to obtain improved constraints on models of charged particle production in hard processes, the study is extended to measurements of pseudorapidity densities of primary charged particles with transverse momenta $p_T > p_T^{cut}$, where $p_T^{cut} = 0.15, 0.5, 1$, or 2 GeV/c, for different inelastic pp collision classes with at least one charged particle in $|\eta| < 0.8$ with a p_T larger than the corresponding threshold p_T^{cut} at $\sqrt{s} = 5.02$ and 13 TeV. The four event classes associated with the different p_T thresholds are identified as INEL>0$_{p_T>0.15}^{|\eta|<0.8}$, INEL>0$_{p_T>0.5}^{|\eta|<0.8}$, INEL>0$_{p_T>1}^{|\eta|<0.8}$, and INEL>0$_{p_T>2}^{|\eta|<0.8}$. These measurements are an extension of the previous studies at LHC Run 1 collision energies ($\sqrt{s} = 0.9$ and 7 TeV) [22]. The p_T threshold of 0.15 GeV/c is chosen to allow comparisons to ALICE results at lower $\sqrt{s}$ while the 0.5 GeV/c threshold allows comparisons with ATLAS and CMS results [23–25]. The higher thresholds of 1 and 2 GeV/c enable the study of particle production with harder particles.

The article is organised as follows. Section 2 addresses the experimental conditions and data samples used in the analysis. Then, the analysis procedures to measure the primary charged particle production and the applied corrections are explained in Sec. 3. Section 4 describes the systematic uncertainties while the results compared to those of ATLAS and CMS and to model predictions are presented in Sec. 5. A brief summary and conclusions are given in Sec. 6.

2 Experimental conditions and data collection

The data samples used in this analysis were collected during LHC Run 2. A sample of 4.4×10^6 minimum bias events in pp collisions at $\sqrt{s} = 5.02$ TeV was used for measurements without a p_T threshold. For measurements requiring a minimum track p_T, samples of 2.5×10^8 and 2.8×10^7 minimum bias events in pp collisions at $\sqrt{s} = 5.02$ and 13 TeV, respectively, were analysed.

Detailed information about the ALICE detector and its performance during LHC Run 2 can be found in Refs. [26] and [27]. Tracking of charged particles is mainly performed with the Inner Tracking System (ITS) [28] and Time Projection Chamber (TPC) [27] located inside a large solenoid that produces a homogeneous magnetic field of 0.5 T directed along the beam direction (z axis in the ALICE reference frame).

The detector closest to the interaction point is the ITS which is composed of 6 cylindrical layers of high resolution silicon detectors. The innermost two layers consist of the Silicon Pixel Detector (SPD) [29, 30]. The SPD layers are coaxial to the beam line with radii of 3.9 and 7.6 cm covering the pseudorapidity range $|\eta| < 2$ for the first layer and $|\eta| < 1.4$ for the second layer. An enlarged pseudorapidity coverage of $|\eta| < 2$ is reached using events whose primary vertex along the beam direction (z_{vtx}) is within ± 10 cm from the nominal interaction point ($z_{vtx} = 0$). Counting the number of tracks for analysis without a p_T threshold (INEL, NSD, INEL>0) relies on the reconstruction of tracklets, which are track segments connecting hits on the two SPD layers and pointing to the primary vertex. Due to the bending of particle trajectories in the magnetic field and multiple scattering, the reconstruction efficiency limits their measurements to $p_T > 50$ MeV/c [19].

The TPC [27], located outside the ITS, is a 90 m^3 cylindrical drift chamber. The TPC covers the pseudorapidity range $|\eta| < 0.9$ with respect to $z = 0$ and the full azimuthal angle. It provides excellent momentum and spatial resolutions for tracking of charged particles. The V0 detector [31] consists of two scintillator arrays that are located on each side of the interaction point along the beam direction and cover the pseudorapidity regions $-3.7 < \eta < -1.7$ (V0C) and $2.8 < \eta < 5.1$ (V0A). It is used for triggering and event selection.

To select different event classes, the SPD and the V0 detectors are used. For the measurements of $dN_{ch}/d\eta$ in INEL, NSD, and INEL>0 events, the minimum-bias trigger requires a hit in the SPD or in either one of the V0 arrays. For the analyses requiring a minimum p_T threshold, the minimum-bias trigger requires signals in both sides of the V0. The SPD and V0 detectors are also used to suppress background from beam–gas collisions and other machine-induced backgrounds. The contamination from background events is removed offline by using the timing difference between the signals in the V0A and V0C detectors [27], exploiting the V0 time resolution which is better than 1 ns. Background events are also rejected by exploiting the correlation between the number of clusters on both layers of the SPD and the number of tracklets in the SPD.

Another type of event background comes from pileup, happening when multiple collisions occur in the same bunch crossing. The overall probability of pileup in ALICE is around 10^{-3} in the minimum-bias pp samples used for these analyses [19]. Pileup contamination is reduced by rejecting events with multiple interaction vertices reconstructed from SPD tracklets. The remaining undetected pileup is negligible in the data samples considered for the analysis presented in this article.

The position of the interaction vertex is obtained using two different approaches: the first is based on the hits in the two SPD layers, the second utilises global tracks that are reconstructed in the TPC and matched to ITS clusters. The primary vertex position is required to be in $|z_{vtx}| < 10$ cm for both inclusive and p_T threshold $dN_{ch}/d\eta$ studies.

3   Analysis procedure and corrections

The measurements of $dN_{ch}/d\eta$ in the event classes without a p_T threshold (INEL, NSD, INEL>0) are based on the tracklet counting method which was used for previous inclusive $dN_{ch}/d\eta$ measurements [16–20]. For SPD tracklets, the association to the position of the primary vertex of the collision is ensured through a χ^2 requirement. By using the interaction point reconstructed with the SPD as the origin, differences in the azimuthal ($\Delta\varphi$, bending plane) and polar ($\Delta\theta$, non-bending direction) angles of two hits, one in the inner and one in the outer SPD layer, are calculated. The tracklets are selected with the following quality cut

$$\chi^2 = \frac{(\Delta\varphi)^2}{\sigma_\varphi^2} + \frac{1}{\sin^2\left(\frac{\theta_1+\theta_2}{2}\right)} \times \frac{(\Delta\theta)^2}{\sigma_\theta^2} < 1.6, \tag{1}$$

where $\sigma_\varphi = 0.08$ rad, $\sigma_\theta = 0.025$ rad, and θ_1 and θ_2 are the polar angles of the hits in each layer of the SPD [19].

To select primary charged particles for the results with p_T thresholds, tracks reconstructed using the hits in the ITS and TPC (global tracks) [26] allow for counting and momentum measurements of charged particles in ALICE. High quality tracks are selected by requiring tracks to have at least 70 (out of maximally 159) crossed pad rows in the TPC, have a good quality of the track momentum fit ($\chi^2/\text{ndf} < 2$), have a distance of closest approach to the primary vertex along the z direction (DCA$_z$) lower than 2 cm, and have a transverse DCA (DCA$_{xy}$) less than 7σ (standard deviations) where σ is p_T-dependent.

All corrections are calculated using Monte Carlo events generated with PYTHIA 6 with the Perugia 2011 tuning [8, 12] or PYTHIA 8 with the Monash 2013 tuning [8, 13–15] event generators with particle transport performed via a GEANT3 [32] simulation of the ALICE detector. Three different Monte Carlo corrections are applied to the raw dN_{ch}/dη: (a) a track-to-particle correction that accounts for detector inefficiencies and background particles like secondaries from interactions in the detector material and decays of primary charged particles including the strange particle content correction, (b) a vertex reconstruction efficiency correction for triggered events without a reconstructed vertex, and (c) a trigger efficiency correction, which accounts for the bias due to the trigger requirement for the corresponding event class. All the track-to-particle corrections are applied as a function of z_{vtx} in order to consider z-dependent dN_{ch}/dη efficiency.

The ALICE definition of primary charged particles excludes particles originating from weak decays of strange particles. Therefore, data have to be corrected for cases when daughter particles from these decays pass the track selection. The strangeness content in data is 40–50% larger than in PYTHIA 6 and PYTHIA 8 [33] in both inclusive and p_T-threshold analyses. This discrepancy is accounted for by scaling the strangeness content in the Monte Carlo simulation to that in the data. The scaling factor is determined by measuring the ratio between the abundance of decay products in $|\eta| < 0.8$ from reconstructed K_s^0, Λ, and $\bar{\Lambda}$ in data and Monte Carlo simulations. The corresponding correction results in a contamination correction of about -0.5% on the final dN_{ch}/dη.

The results of dN_{ch}/dη for INEL and NSD events are affected by the model uncertainty for diffractive events. Cross section measurements with ALICE indicate that the number of single-diffractive (SD) and double-diffractive (DD) events are about 20% and 12% of the number of inelastic events, respectively, at both $\sqrt{s} = 2.76$ and 7 TeV [34]. As for the previous ALICE measurements of dN_{ch}/dη for the INEL, NSD, and INEL>0 event classes [19], a special PYTHIA 6 tune for diffraction is used [34]. For this tune, the diffractive mass distribution of SD events is re-weighted while the one of DD events is unchanged. For a consistent treatment, the mass distribution of SD events in both event generators (PYTHIA 6 Perugia 2011 and PYTHIA 8 Monash 2013) are re-weighted to follow those used in the special PYTHIA 6 tune. Note that both the INEL>0 and p_T^{cut} analyses do not contain single diffractive events due to the requirement of at least one charged particle at midrapidity. Therefore, the tuning procedure for the SD diffraction mass in the event generator is not required.

4   Systematic uncertainties

Several sources of systematic uncertainties were investigated. For the tracklet analysis at $\sqrt{s} = 5.02$ TeV, the uncertainty related to the contribution of SD/DD events was evaluated by varying the fractions of SD and DD processes produced by PYTHIA 8 by $\pm 50\%$ of their nominal values. The result of dN_{ch}/dη corrected by a track-to-particle correction map implementing the re-weighted SD mass distribution is used to determine the central values of the minimum-bias events. Results with a two-times steeper re-weighted mass distribution and the default mass distribution in models were used to estimate the systematic uncertainty coming from the unknown SD mass distribution [34]. The highest deviation was taken as a systematic uncertainty. The third dominant source of uncertainty, which applies only to the tracklet analysis, includes the extrapolation of the number of particles as a function of p_T from 50 MeV/c down to zero, where the SPD is insensitive. The number of primary charged particles in this low p_T

Table 1: Relative values of systematic uncertainties (expressed in %) on $dN_{ch}/d\eta$ at $\eta = 0$ for INEL, NSD, and INEL>0 event classes determined in pp collisions at $\sqrt{s} = 5.02$ TeV.

Source of uncertainty	Systematic uncertainty at $\eta = 0$ (%)		
	INEL	NSD	INEL>0
Diffraction ratio	± 4.5	± 2	± 0.1
Diffraction shape	$+3$	-0.2	-0.2
Zero-p_T extrapolation	$+1, -0.5$	$+1, -0.5$	$+1, -0.5$
Event generator dependence	± 0.2	± 1	± 0.4
Acceptance and efficiency	± 0.8	± 0.8	± 0.8
z_{vtx} dependence	± 0.3	± 0.3	± 0.3
Strangeness enhancement factor	± 0.5	± 0.5	± 0.5
Particle composition	± 0.4	± 0.4	± 0.4
Material budget	± 0.2	± 0.2	± 0.2
Total systematic uncertainty	$+5.5, -4.6$	$+2.5, -2.3$	$+1.2, -1.1$

Table 2: Relative values of systematic uncertainties (expressed in %) on $dN_{ch}/d\eta$ at $\eta = 0$ for INEL>0$_{p_T>0.15}^{|\eta|<0.8}$, INEL>0$_{p_T>0.5}^{|\eta|<0.8}$, INEL>0$_{p_T>1}^{|\eta|<0.8}$, and INEL>0$_{p_T>2}^{|\eta|<0.8}$ event classes determined in pp collisions at $\sqrt{s} = 5.02$ and 13 TeV.

Source of uncertainty	Systematic uncertainty at $\eta = 0$ (%)							
	INEL>0$_{p_T>0.15}^{|\eta|<0.8}$		INEL>0$_{p_T>0.5}^{|\eta|<0.8}$		INEL>0$_{p_T>1}^{|\eta|<0.8}$		INEL>0$_{p_T>2}^{|\eta|<0.8}$	
$\sqrt{s}$ (TeV)	5.02	13	5.02	13	5.02	13	5.02	13
Track selection	± 2.0	± 2.0	± 2.5	± 2.3	± 1.8	± 1.8	± 1.4	± 0.9
Event generator dependence	± 1	± 0.9	± 1.2	± 1.3	± 2	± 1.9	± 2	± 1.7
Acceptance and efficiency	± 1	± 0.5	± 1	± 0.6	± 1.3	± 0.7	± 1.8	± 1.8
z_{vtx} dependence	± 0.3	± 0.2	± 0.3	± 0.3	± 0.3	± 0.3	± 0.5	± 0.5
Strangeness enhancement factor	± 0.3	± 0.3	± 0.3	± 0.2	± 0.1	± 0.1	neg.	neg.
Particle composition	± 0.8	± 0.7	± 0.8	± 0.8	± 1	± 1	± 1.8	± 1.6
Material budget	± 0.2	± 0.2	± 0.2	± 0.2	± 0.2	± 0.2	± 0.2	± 0.2
Total systematic uncertainty	± 2.6	± 2.4	± 3.1	± 2.9	± 3.2	± 2.9	± 3.6	± 3.1

range is varied conservatively in the event generator by $+100\%$ and -50%, adopted from the previous study [19]. The corresponding uncertainty is found to be $+1\%$ and -0.5% consistently, for the three event classes.

For the analyses with a minimum p_T threshold, the uncertainty due to the track selection is estimated by varying all the criteria around their nominal values. Three more sets of track selection criteria called tight- and loose-cut global tracks, and hybrid tracks [35] are considered in this study. The tight- and loose-cut global tracks are selected by tightening and loosening the DCA cuts with respect to the primary vertex, respectively. Hybrid tracks are composed of two track classes. The first class consists of tracks that have at least one hit in the SPD. The tracks from the second class do not have any SPD associated hit and, hence, use the primary vertex as the innermost constraint for the tracking. The selection of hybrid tracks ensures a uniform distribution of tracks as a function of azimuthal angle. This systematic uncertainty contribution increases from 2.8% to 5% with increasing p_T^{cut} and is slightly larger for the results at $\sqrt{s} =$ 5.02 TeV.

All other sources of uncertainty were estimated in the same way for tracklets and global tracks; all values can be found in Tables 1 and 2. The systematic uncertainty from the event generator dependence was also included. Data were corrected with PYTHIA 6 [8, 12] and the relative deviation of the final result corrected with PYTHIA 8 was assigned as a systematic uncertainty. The uncertainty on the detector acceptance and efficiency was estimated by measuring $dN_{ch}/d\eta$ for three different azimuthal regions and comparing it to the measurement in the whole region. The uncertainty due to the acceptance was studied additionally by dividing the whole event sample into 10 different intervals of the primary vertex position within $z_{vtx} = \pm 10$ cm, each having the same number of events and performing the same analysis in each interval. The material budget in the ALICE central barrel is known to a precision of about 4% [30]. The corresponding systematic uncertainty, obtained by varying the material budget in the simulation, is estimated to be 0.2%. The uncertainty associated with the correction for the difference in strange particle content between data and MC was estimated by varying the strange particle content in the simulation. The yield of strange particles in data as compared to the simulation was measured as a function of p_T to be up to a factor 1.5 different and this factor was varied by $\pm 30\%$. Additionally, the particle composition affects the efficiency estimate because different particle species have different efficiencies that depend on the applied effective p_T cut-offs and the decay kinematics. The influence of this uncertainty was estimated by varying, in the simulation, the relative fraction of charged kaons, protons, and antiprotons with respect to charged pions by $\pm 30\%$.

The systematic uncertainties due to the event generator dependence, acceptance and efficiency, and z_{vtx} dependence are treated as uncorrelated while the ones for the diffraction tuning (inclusive study only), zero-p_T extrapolation (inclusive study only), strange particle abundance, particle composition, track se- lection (p_T threshold study only), and material budget are correlated between η bins in Fig. 1, 3, and 4. Note that the statistical uncertainties in these analyses are negligible.

5   Results

The measurements of $dN_{ch}/d\eta$ as a function of η at $\sqrt{s} = 5.02$ TeV for INEL, NSD, and INEL>0 events are shown in Fig. 1. The distributions of $dN_{ch}/d\eta$ are compared to PYTHIA 6 with the Perugia 2011 tuning and PYTHIA 8 with the Monash 2013 tuning for the same event classes. In general, the models are better at describing the distributions which contain a smaller contribution from diffractive interactions. Therefore, the NSD and INEL>0 event classes are described by models well. This can also be seen in the bottom panels of Fig. 1 where the relative difference between models and data for the INEL event class stays within 10% and for the NSD and INEL>0 event classes stay within 5%.

The predictions of the two PYTHIA versions are very similar, however PYTHIA 6 shows a better agree- ment with data for the INEL event class. The values of the charged particle pseudorapidity density
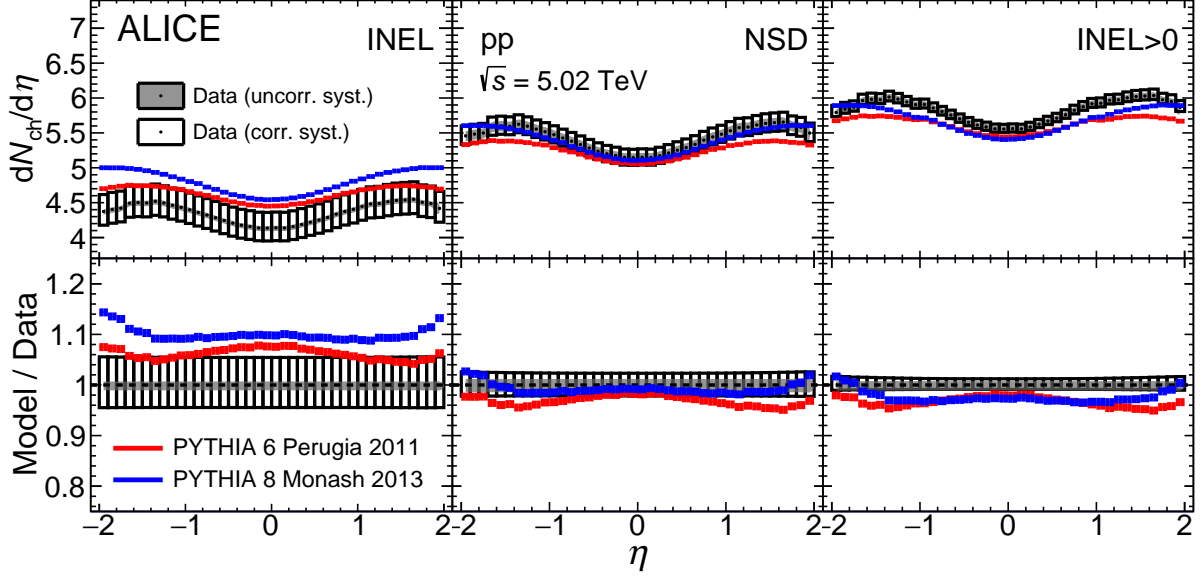
Figure 1: The distributions of dN_{ch}/dη for INEL (left panel), NSD (middle panel), and INEL>0 (right panel) event classes in pp collisions at $\sqrt{s}$ = 5.02 TeV. Data are compared to simulations obtained with PYTHIA 6 with the Perugia 2011 tuning and PYTHIA 8 with the Monash 2013 tuning. Grey bands (unfilled rectangles) represent the uncorrelated (correlated) systematic uncertainties from data. The bottom part of the figure shows the ratios between models and data.

averaged over $|\eta| < 0.5$ and $|\eta| < 1$ ($\langle$dN_{ch}/d$\eta\rangle$) are reported in Table 3. The $\langle$dN_{ch}/d$\eta\rangle$ values are provided for the INEL, NSD, and INEL>0 event classes. The values obtained from the PYTHIA event generators are also reported.

Table 3: The average dN_{ch}/dη ($\langle$dN_{ch}/d$\eta\rangle$) in INEL, NSD, and INEL>0 in pp collisions at $\sqrt{s}$ = 5.02 TeV.

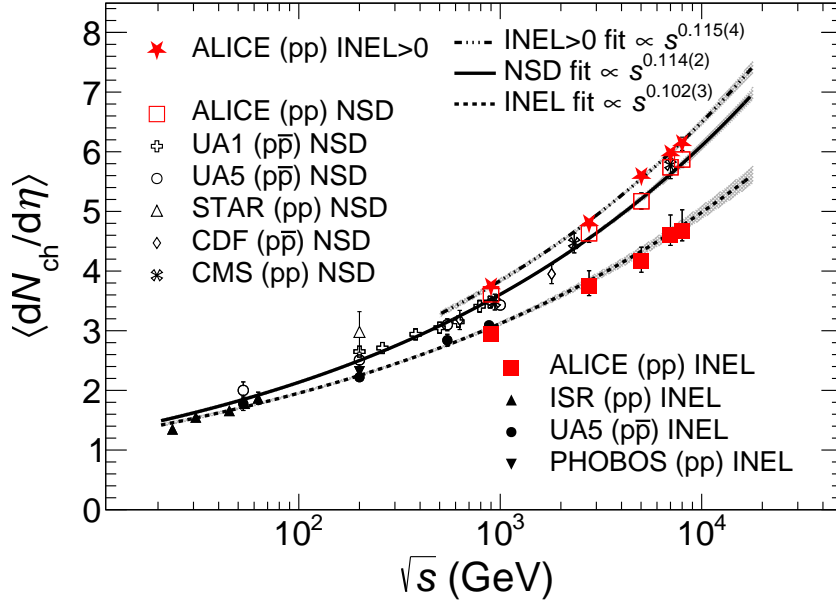| Event class | $\langle$dN_{ch}/d$\eta\rangle$ | | | | | |
| | Data±syst. | | PYTHIA 6 Perugia 2011 | | PYTHIA 8 Monash 2013 | |
	$|\eta| < 0.5$	$|\eta| < 1$	$|\eta| < 0.5$	$|\eta| < 1$	$|\eta| < 0.5$	$|\eta| < 1$
INEL	$4.17^{+0.23}_{-0.19}$	$4.25^{+0.23}_{-0.19}$	4.48	4.54	4.58	4.65
NSD	$5.18^{+0.14}_{-0.13}$	$5.28^{+0.13}_{-0.12}$	5.09	5.16	5.14	5.23
INEL>0	$5.60^{+0.08}_{-0.08}$	$5.70^{+0.08}_{-0.07}$	5.48	5.55	5.44	5.54

Figure 2 shows the values of $\langle$dN_{ch}/d$\eta\rangle$ averaged over $|\eta| < 0.5$ for the INEL, NSD, and INEL>0 event classes as a function of the centre-of-mass energy after combining the ALICE data with other data at the LHC and at lower energies [19, 36–43]. It is worth mentioning that the result for the INEL event class can be compared with the results in Pb–Pb and p–Pb collisions at the same centre-of-mass energies [44, 45]. At midrapidity, the measured dN_{ch}/dη can be parameterised by a power-law fit as dN_{ch}/d$\eta \propto s^{\delta}$, resulting in $\delta = 0.102 \pm 0.003$, 0.114 ± 0.003, and 0.115 ± 0.004 for INEL, NSD, and INEL>0 events, respectively. The energy dependence of particle production shows that the power-law fit is still valid. These results can be compared to $\delta = 0.153 \pm 0.002$ for central heavy-ion (A–A) collisions [46, 47]. This shows that the primary charged particle pseudorapidity density increases faster with energy in central A–A collisions compared to pp collisions, indicating that the initial longitudinal energy is more efficiently converted into particles in heavy-ion collisions relative to pp and p–Pb collisions.

The measurements of dN_{ch}/dη as a function of η at $\sqrt{s}$ = 5.02 and 13 TeV are shown in Figs. 3 and 4, for the INEL>0$^{|\eta|<0.8}_{p_T>0.15}$, INEL>0$^{|\eta|<0.8}_{p_T>0.5}$, INEL>0$^{|\eta|<0.8}_{p_T>1}$, and INEL>0$^{|\eta|<0.8}_{p_T>2}$ event classes. The results are also

Figure 2: The values of $\langle \mathrm{d}N_{\mathrm{ch}}/\mathrm{d}\eta \rangle$ averaged over $|\eta| < 0.5$ for the INEL, NSD, and INEL>0 event classes as a function of centre-of-mass energy [19, 36–43]. The lines indicate a power-law fit for each event class. The grey bands show one standard deviation of the fit.

compared to the predictions from the PYTHIA 8 with the Monash 2013 tuning and EPOS LHC event generators, where EPOS LHC was tuned on LHC Run 1 data at lower $\sqrt{s}$ [9]. In general, the largest disagreement between data and MC is observed for the softest (INEL>0$^{|\eta|<0.8}_{p_T>0.15}$) and hardest (INEL>0$^{|\eta|<0.8}_{p_T>2}$) event classes. For collisions at $\sqrt{s} = 5.02$ TeV, EPOS LHC describes the data to within 2% in the measured η range for all event classes, while PYTHIA 8 underestimates the measured $\langle \mathrm{d}N_{\mathrm{ch}}/\mathrm{d}\eta \rangle$ by 4–8% depending on the p_T^{cut}. On the other hand, at $\sqrt{s} = 13$ TeV, PYTHIA 8 provides a better description of the measurements as compared to EPOS LHC. At the highest collision energy, PYTHIA 8 predictions are consistent with the data within the uncertainties, while EPOS LHC undershoots the data by 4–10% depending on the event class. The results are expected to provide better constraints on charged particle production mechanisms implemented in models affecting both soft and hard QCD and their energy dependence.

The left panel of Fig. 5 shows the results for the INEL>0$^{|\eta|<0.8}_{p_T>0.5}$ event class extrapolated to the pseudorapidity interval $|\eta| < 2.5$ to compare them to the ATLAS results [24]. The normalisation factor is computed as the ratio of the $\mathrm{d}N_{\mathrm{ch}}/\mathrm{d}\eta$ for the INEL>0$^{|\eta|<0.8}_{p_T>0.5}$ and INEL>0$^{|\eta|<2.5}_{p_T>0.5}$ event classes obtained from PYTHIA 8 Monash 2013 simulations. This normalisation is needed to do a correct comparison among different experiments because the condition with at least one charged particle depends on the acceptance. When experimentally the INEL>0 condition is requested with a wider pseudorapidity acceptance, the corresponding event class is more inclusive because it collects more soft events. In the right panel of Fig. 5, the same procedure is applied to normalise to the INEL>0$^{|\eta|<2.4}_{p_T>0.5}$ event class in order to compare the result from ALICE to that obtained by CMS [?]. The result of ALICE is larger than those of ATLAS by $\sim 3\%$ and CMS by up to $\sim 2\%$. However, they are compatible within systematic uncertainties.

6 Conclusions

This article presents a set of measurements of the pseudorapidity density of primary charged particles ($\mathrm{d}N_{\mathrm{ch}}/\mathrm{d}\eta$) in proton–proton collisions at centre-of-mass energies $\sqrt{s} = 5.02$ and 13 TeV. Results for inelastic (INEL) and non-single-diffractive (NSD) events as well as for inelastic events having at least
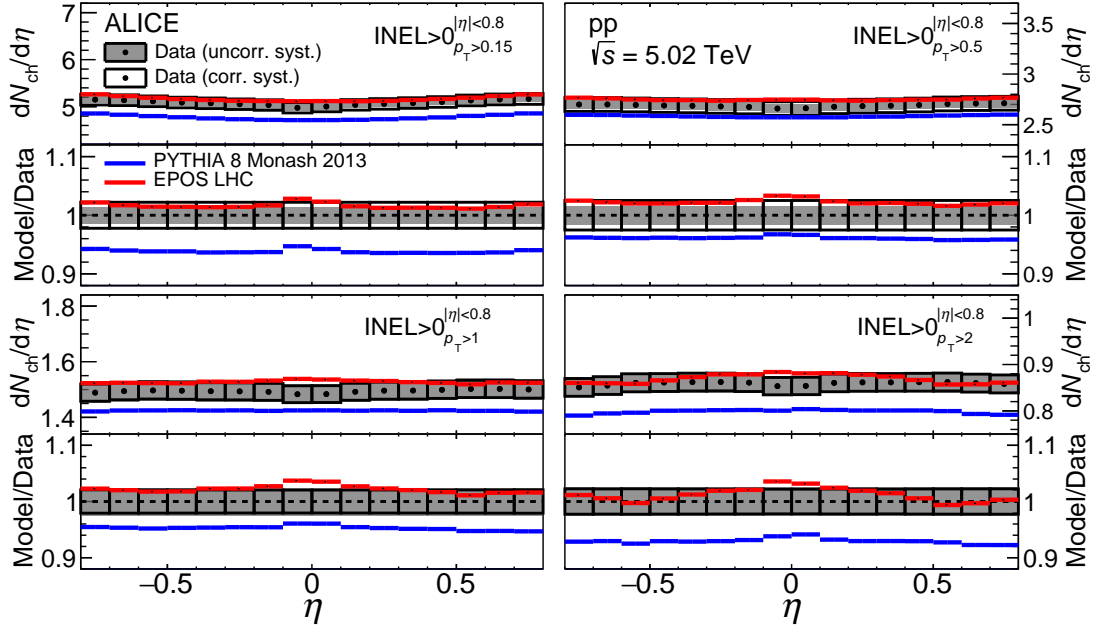
Figure 3: Pseudorapidity density distributions of charged particles, $dN_{ch}/d\eta$, in pp collisions at $\sqrt{s} = 5.02$ TeV for the four event classes, INEL>0$^{|\eta|<0.8}_{p_T>0.15}$, INEL>0$^{|\eta|<0.8}_{p_T>0.5}$, INEL>0$^{|\eta|<0.8}_{p_T>1}$, and INEL>0$^{|\eta|<0.8}_{p_T>2}$, compared to the distributions from models: PYTHIA 8 Monash 2013 and EPOS LHC. Grey bands (unfilled rectangles) represent the uncorrelated (correlated) systematic uncertainties from data.
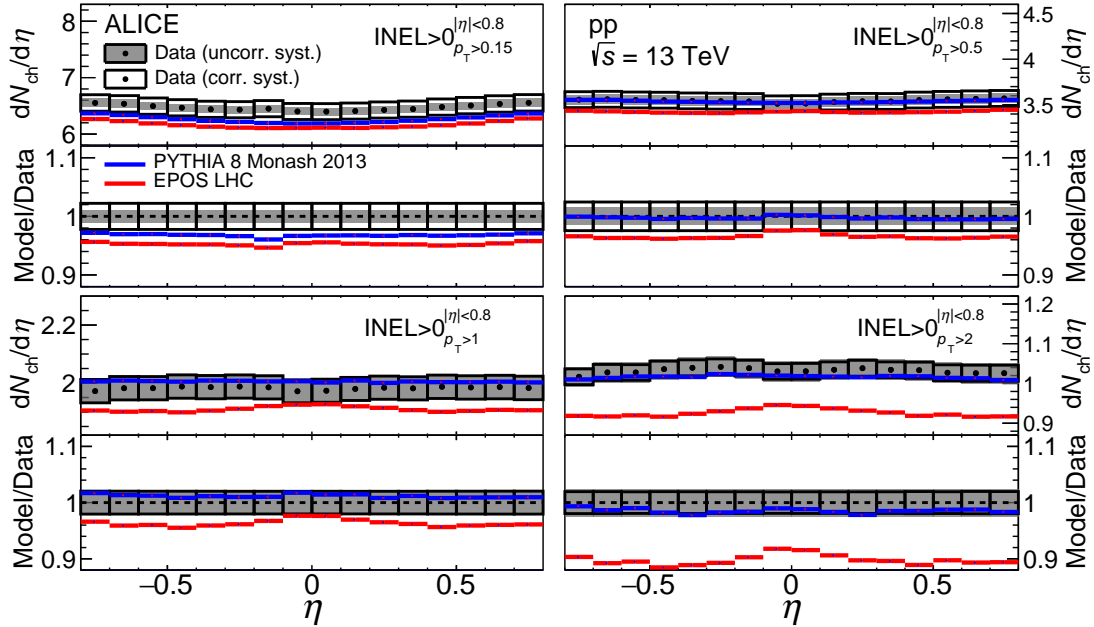

Figure 4: Pseudorapidity density distributions of charged particles, $dN_{ch}/d\eta$, in pp collisions at $\sqrt{s} = 13$ TeV for the four event classes, INEL>0$^{|\eta|<0.8}_{p_T>0.15}$, INEL>0$^{|\eta|<0.8}_{p_T>0.5}$, INEL>0$^{|\eta|<0.8}_{p_T>1}$, and INEL>0$^{|\eta|<0.8}_{p_T>2}$, compared to the distributions from models: PYTHIA 8 Monash 2013 and EPOS LHC. Grey bands (unfilled rectangles) represent the uncorrelated (correlated) systematic uncertainties from data.
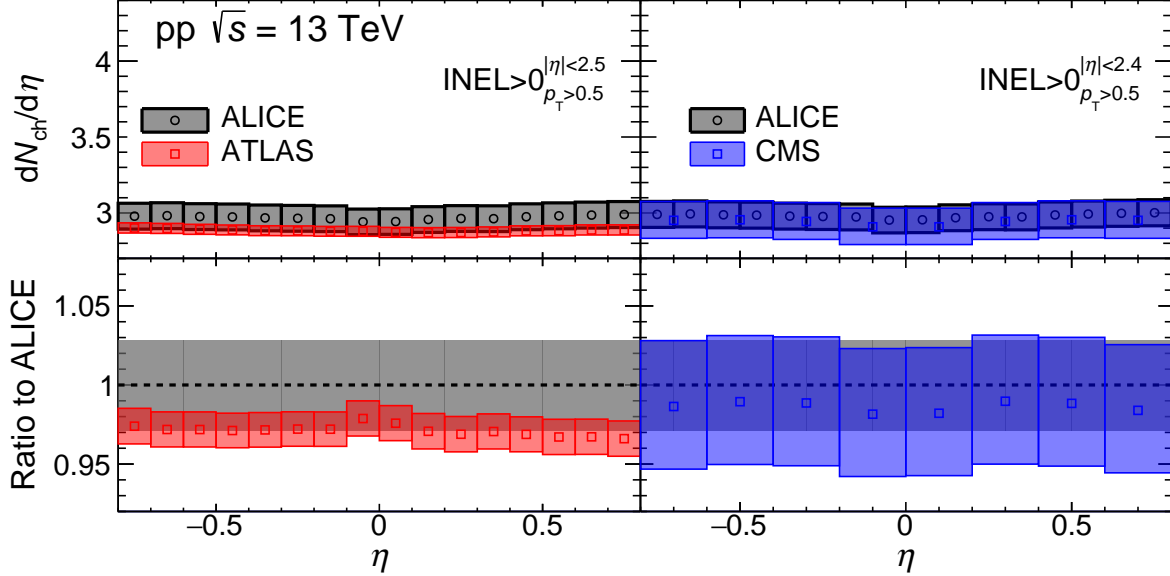
Figure 5: The distributions of $dN_{ch}/d\eta$ for the INEL>$0^{|\eta|<0.8}_{p_T>0.5}$ event class are normalised to the (a) INEL>$0^{|\eta|<2.5}_{p_T>0.5}$ and (b) INEL>$0^{|\eta|<2.4}_{p_T>0.5}$ event classes using PYTHIA 8 with the Monash 2013 tuning in pp collisions at $\sqrt{s} = 13$ TeV [24?]. The bottom panels show the ratio of $dN_{ch}/d\eta$ for the INEL>$0^{|\eta|<2.5}_{p_T>0.5}$ (left) and INEL>$0^{|\eta|<2.4}_{p_T>0.5}$ (right) event class between ALICE and ATLAS (left) and between ALICE and CMS (right), respectively.

one charged particle produced in the pseudorapidity interval $|\eta| < 1$ (INEL>0) are presented specifically at $\sqrt{s} = 5.02$ TeV. The predictions of PYTHIA 6 with the Perugia 2011 tuning and PYTHIA 8 with the Monash 2013 tuning are close to each other. The two models show agreement with data except for the case of the NSD event class. Also, the result of the INEL event class is not well described by models due to the higher diffractive content.

The values of the average pseudorapidity density $\langle dN_{ch}/d\eta \rangle$ in $|\eta| < 0.5$ for INEL, NSD, and INEL>0 events with an in-depth study for the single and double diffractive contributions are reported: $4.17^{+0.23}_{-0.19}$, $5.18^{+0.14}_{-0.13}$ and $5.60^{+0.08}_{-0.08}$ with systematic uncertainties, respectively. The energy dependence of $\langle dN_{ch}/d\eta \rangle$ is updated with the new values at $\sqrt{s} = 5.02$ TeV and then it is parameterised by a power-law fit as $\langle dN_{ch}/d\eta \rangle \propto s^\delta$, resulting in $\delta = 0.102 \pm 0.003$, 0.114 ± 0.003, and 0.115 ± 0.004 for INEL, NSD, and INEL>0 events, respectively.

To provide detailed constraints on the charged particle production with hard processes in pp collisions at $\sqrt{s} = 5.02$ and 13 TeV, the study is extended with the pseudorapidity density of primary charged particles in the pseudorapidity interval $|\eta| < 0.8$ with minimum transverse momentum thresholds of $p_T = 0.15$, 0.5, 1, and 2 GeV/c that are called INEL>$0^{|\eta|<0.8}_{p_T>0.15}$, INEL>$0^{|\eta|<0.8}_{p_T>0.5}$, INEL>$0^{|\eta|<0.8}_{p_T>1}$, and INEL>$0^{|\eta|<0.8}_{p_T>2}$, respectively. The results of the $dN_{ch}/d\eta$ distributions are also compared to the predictions from the PYTHIA 8 with the Monash 2013 tuning and EPOS LHC event generators. PYTHIA 8 tends to underestimate the overall distributions at $\sqrt{s} = 5.02$ TeV by up to 8%, while EPOS LHC undershoots the measured multiplicities by up to 10% as the p_T threshold increases at $\sqrt{s} = 13$ TeV. The largest disagreement between data and MC is observed for the softest (INEL>$0^{|\eta|<0.8}_{p_T>0.15}$) and hardest (INEL>$0^{|\eta|<0.8}_{p_T>2}$) event classes indicating the importance of these measurements to constrain models.

In order to compare the ALICE result with minimum p_T thresholds to those from the ATLAS and CMS experiments, the INEL>$0^{|\eta|<0.8}_{p_T>0.5}$ measurement is normalised to the INEL>$0^{|\eta|<2.5}_{p_T>0.5}$ and INEL>$0^{|\eta|<2.4}_{p_T>0.5}$ event classes, respectively, using PYTHIA 8. The ALICE measurements agree with those from the other

LHC experiments within systematic uncertainties.

References

[1] R. D. Field and R. P. Feynman, "Quark Elastic Scattering as a Source of High Transverse Momentum Mesons", *Phys. Rev. D* **15** (1977) 2590–2616.

[2] M. Srednicki, *Quantum field theory*. Cambridge University Press, 1, 2007.

[3] P. D. B. Collins, *An Introduction to Regge Theory and High-Energy Physics*. Cambridge Monographs on Mathematical Physics. Cambridge Univ. Press, Cambridge, UK, 5, 2009.

[4] W. Greiner, S. Schramm, and E. Stein, *Quantum chromodynamics*. 2002.

[5] S. Ostapchenko, "Status of QGSJET", *AIP Conf. Proc.* **928** (2007) 118–125, `arXiv:0706.3784 [hep-ph]`.

[6] R. S. Fletcher, T. K. Gaisser, P. Lipari, and T. Stanev, "SIBYLL: An Event generator for simulation of high-energy cosmic ray cascades", *Phys. Rev. D* **50** (1994) 5710–5731.

[7] R. Engel, "Photoproduction within the two component dual parton model. 1. Amplitudes and cross-sections", *Z. Phys. C* **66** (1995) 203–214.

[8] T. Sjostrand, S. Mrenna, and P. Z. Skands, "PYTHIA 6.4 Physics and Manual", *JHEP* **05** (2006) 026, `arXiv:hep-ph/0603175 [hep-ph]`.

[9] T. Pierog, I. Karpenko, J. M. Katzy, E. Yatsenko, and K. Werner, "EPOS LHC: Test of collective hadronization with data measured at the CERN Large Hadron Collider", *Phys. Rev. C* **92** (2015) 034906, `arXiv:1306.0121 [hep-ph]`.

[10] M. Bahr *et al.*, "Herwig++ Physics and Manual", *Eur. Phys. J. C* **58** (2008) 639–707, `arXiv:0803.0883 [hep-ph]`.

[11] T. Gleisberg, S. Hoeche, F. Krauss, M. Schonherr, S. Schumann, F. Siegert, and J. Winter, "Event generation with SHERPA 1.1", *JHEP* **02** (2009) 007, `arXiv:0811.4622 [hep-ph]`.

[12] P. Z. Skands, "Tuning Monte Carlo Generators: The Perugia Tunes", *Phys. Rev. D* **82** (2010) 074018, `arXiv:1005.3457 [hep-ph]`.

[13] T. Sjostrand, S. Mrenna, and P. Z. Skands, "A Brief Introduction to PYTHIA 8.1", *Comput.Phys.Commun.* **178** (2008) 852–867, `arXiv:0710.3820 [hep-ph]`.

[14] T. Sjöstrand *et al.*, "An introduction to PYTHIA 8.2", *Comput. Phys. Commun.* **191** (2015) 159–177, `arXiv:1410.3012 [hep-ph]`.

[15] P. Skands, S. Carrazza, and J. Rojo, "Tuning PYTHIA 8.1: the Monash 2013 Tune", *Eur. Phys. J. C74* (2014) 3024, `arXiv:1404.5630 [hep-ph]`.

[16] **ALICE** Collaboration, K. Aamodt *et al.*, "First proton-proton collisions at the LHC as observed with the ALICE detector: Measurement of the charged particle pseudorapidity density at $\sqrt{s} = 900$ GeV", *Eur. Phys. J. C* **65** (2010) 111–125, `arXiv:0911.5430 [hep-ex]`.

[17] **ALICE** Collaboration, K. Aamodt *et al.*, "Charged-particle multiplicity measurement in proton-proton collisions at $\sqrt{s} = 0.9$ and 2.36 TeV with ALICE at LHC", *Eur. Phys. J. C* **68** (2010) 89–108, `arXiv:1004.3034 [hep-ex]`.

[18] **ALICE** Collaboration, K. Aamodt *et al.*, "Charged-particle multiplicity measurement in proton-proton collisions at $\sqrt{s} = 7$ TeV with ALICE at LHC", *Eur. Phys. J. C* **68** (2010) 345–354, `arXiv:1004.3514 [hep-ex]`.

[19] **ALICE** Collaboration, J. Adam *et al.*, "Charged-particle multiplicities in proton–proton collisions at $\sqrt{s} = 0.9$ to 8 TeV", *Eur. Phys. J. C* **77** (2017) 33, `arXiv:1509.07541 [nucl-ex]`.

[20] **ALICE** Collaboration, J. Adam *et al.*, "Pseudorapidity and transverse-momentum distributions of charged particles in proton–proton collisions at $\sqrt{s} = 13$ TeV", *Phys. Lett. B* **753** (2016) 319–329, `arXiv:1509.08734 [nucl-ex]`.

[21] **ALICE** Collaboration, "The ALICE definition of primary particles", *ALICE-PUBLIC-NOTE-2017-005* (2017) . `https://cds.cern.ch/record/2270008`.

[22] **ALICE** Collaboration, "Charged-particle multiplicity measurement with Reconstructed Tracks in pp Collisions at $\sqrt{s} = 0.9$ and 7 TeV with ALICE at the LHC", *ALICE-PUBLIC-2013-001* (7, 2013) .

[23] **ATLAS** Collaboration, G. Aad *et al.*, "Charged-particle multiplicities in pp interactions measured with the ATLAS detector at the LHC", *New J. Phys.* **13** (2011) 053033, `arXiv:1012.5104 [hep-ex]`.

[24] **ATLAS** Collaboration, G. Aad *et al.*, "Charged-particle distributions in $\sqrt{s} = 13$ TeV pp interactions measured with the ATLAS detector at the LHC", *Phys. Lett. B* **758** (2016) 67–88, `arXiv:1602.01633 [hep-ex]`.

[25] **CMS** Collaboration, A. M. Sirunyan *et al.*, "Measurement of charged particle spectra in minimum-bias events from proton–proton collisions at $\sqrt{s} = 13\,\mathrm{TeV}$", *Eur. Phys. J. C* **78** (2018) 697, `arXiv:1806.11245 [hep-ex]`.

[26] **ALICE** Collaboration, K. Aamodt *et al.*, "The ALICE experiment at the CERN LHC", *JINST* **3** (2008) S08002.

[27] **ALICE** Collaboration, B. Abelev *et al.*, "Performance of the ALICE Experiment at the CERN LHC", *Int. J. Mod. Phys. A* **29** (2014) 1430044, `arXiv:1402.4476 [nucl-ex]`.

[28] **ALICE** Collaboration, K. Aamodt *et al.*, "Alignment of the ALICE Inner Tracking System with cosmic-ray tracks", *JINST* **5** (2010) P03003, `arXiv:1001.0502 [physics.ins-det]`.

[29] R. Santoro *et al.*, "The ALICE Silicon Pixel Detector: Readiness for the first proton beam", *JINST* **4** (2009) P03023.

[30] **ALICE** Collaboration, B. Abelev *et al.*, "Performance of the ALICE Experiment at the CERN LHC", *Int. J. Mod. Phys.* **A29** (2014) 1430044, `arXiv:1402.4476 [nucl-ex]`.

[31] **ALICE** Collaboration, P. Cortese *et al.*, "ALICE forward detectors: FMD, T0 and V0: Technical Design Report", tech. rep., Geneva, 9, 2004. `https://cds.cern.ch/record/781854`.

[32] Brun *et al.*, *GEANT: Detector Description and Simulation Tool; Oct 1994*. CERN Program Library. CERN, Geneva, 1993. `https://cds.cern.ch/record/1082634`. Long Writeup W5013.

[33] **ALICE** Collaboration, J. Adam *et al.*, "Enhanced production of multi-strange hadrons in high-multiplicity proton-proton collisions", *Nature Phys.* **13** (2017) 535–539, `arXiv:1606.07424 [nucl-ex]`.

[34] **ALICE** Collaboration, B. Abelev *et al.*, "Measurement of inelastic, single- and double-diffraction cross sections in proton–proton collisions at the LHC with ALICE", *Eur. Phys. J. C* **73** (2013) 2456, `arXiv:1208.4968 [hep-ex]`.

[35] **ALICE** Collaboration, B. Abelev *et al.*, "Long-range angular correlations on the near and away side in p–Pb collisions at $\sqrt{s_{NN}}$ = 5.02 TeV", *Phys. Lett.* **B719** (2013) 29–41, `arXiv:1212.2001 [nucl-ex]`.

[36] **UA1** Collaboration, C. Albajar *et al.*, "A Study of the General Characteristics of $p\bar{p}$ Collisions at $\sqrt{s}$ = 0.2 TeV to 0.9 TeV", *Nucl. Phys. B* **335** (1990) 261–287.

[37] **UA5** Collaboration, G. J. Alner *et al.*, "Scaling of Pseudorapidity Distributions at c.m. Energies Up to 0.9 TeV", *Z. Phys. C* **33** (1986) 1–6.

[38] **STAR** Collaboration, B. I. Abelev *et al.*, "Systematic Measurements of Identified Particle Spectra in pp, d+Au and Au+Au Collisions from STAR", *Phys. Rev. C* **79** (2009) 034909, `arXiv:0808.2041 [nucl-ex]`.

[39] **CDF** Collaboration, F. Abe *et al.*, "Pseudorapidity distributions of charged particles produced in $\bar{p}p$ interactions at $\sqrt{s}$ = 630 GeV and 1800 GeV", *Phys. Rev. D* **41** (Apr, 1990) 2330–2333.

[40] **CMS** Collaboration, V. Khachatryan *et al.*, "Transverse-momentum and pseudorapidity distributions of charged hadrons in pp collisions at $\sqrt{s}$ = 7 TeV", *Phys. Rev. Lett.* **105** (2010) 022002, `arXiv:1005.3299 [hep-ex]`.

[41] **CMS** Collaboration, V. Khachatryan *et al.*, "Transverse Momentum and Pseudorapidity Distributions of Charged Hadrons in pp Collisions at $\sqrt{s}$ = 0.9 and 2.36 TeV", *JHEP* **02** (2010) 041, `arXiv:1002.0621 [hep-ex]`.

[42] **Ames-Bologna-CERN-Dortmund-Heidelberg-Warsaw** Collaboration, A. Breakstone *et al.*, "Charged Multiplicity Distribution in p p Interactions at ISR Energies", *Phys. Rev. D* **30** (1984) 528.

[43] **PHOBOS** Collaboration, R. Nouicer *et al.*, "Pseudorapidity distributions of charged particles in d + Au and p + p collisions at $\sqrt{s_{NN}}$ = 200 GeV", *J. Phys. G* **30** (2004) S1133–S1138, `arXiv:nucl-ex/0403033`.

[44] **ALICE** Collaboration, B. Abelev *et al.*, "Pseudorapidity density of charged particles in p–Pb collisions at $\sqrt{s_{NN}}$ = 5.02 TeV", *Phys. Rev. Lett.* **110** (2013) 032301, `arXiv:1210.3615 [nucl-ex]`.

[45] **ALICE** Collaboration, J. Adam *et al.*, "Centrality dependence of the charged-particle multiplicity density at midrapidity in Pb–Pb collisions at $\sqrt{s_{NN}}$ = 5.02 TeV", *Phys. Rev. Lett.* **116** (2016) 222302, `arXiv:1512.06104 [nucl-ex]`.

[46] **ALICE** Collaboration, S. Acharya *et al.*, "Centrality and pseudorapidity dependence of the charged-particle multiplicity density in Xe–Xe collisions at $\sqrt{s_{NN}}$ =5.44 TeV", *Phys. Lett. B* **790** (2019) 35–48, `arXiv:1805.04432 [nucl-ex]`.

[47] S. Basu, S. Thakur, T. K. Nayak, and C. A. Pruneau, "Multiplicity and pseudorapidity density distributions of charged particles produced in pp, pA and AA collisions at RHIC & LHC energies", *J. Phys. G* **48** (2020) 025103, `arXiv:2008.07802 [nucl-ex]`.